Received: 21 November 2018 | Revised: 20 December 2019 | Accepted: 1 January 2020

DOI: 10.1002/wcc.637

OPINION

WIREs CLIMATE CHANGE WILEY

Preserving the coupled atmosphere–ocean feedback in initializations of decadal climate predictions

Sebastian Brune | **Johanna Baehr**

Institute of Oceanography, CEN, Universität Hamburg, Hamburg, Germany

Correspondence
Sebastian Brune, Institute of Oceanography, CEN, Universität Hamburg, Bundesstr. 53, 20146 Hamburg, Germany.
Email: sebastian.brune@uni-hamburg.de

Funding information
Bundesministerium für Bildung und Forschung, Grant/Award Numbers: 01LP1157C, 01LP1516A; Deutsche Forschungsgemeinschaft, Grant/Award Numbers: EXC 177, EXC 2037

Edited by Eduardo Zorita, Domain Editor, and Mike Hulme, Editor-in-Chief

Abstract

On interannual to decadal time scales, memory in the Earth's climate system resides to a large extent in the slowly varying heat content of the ocean, which responds to fast atmospheric variability and in turn sets the frame for large-scale atmospheric circulation patterns. This large-scale coupled atmosphere–ocean feedback is generally well represented in today's Earth system models. This may fundamentally change when data assimilation is used to bring such models close to an observed state to initialize interannual to decadal climate predictions. Here, we review how the large-scale coupled atmosphere–ocean feedback is preserved in common approaches to construct such initial conditions, with the focus on the initialized ocean state. In a set of decadal prediction experiments, ranging from an initialization of atmospheric variability only to full-field nudging of both atmosphere and ocean, we evaluate the variability and predictability of the Atlantic meridional overturning circulation, of the Atlantic multidecadal variability and North Atlantic subpolar gyre sea surface temperatures. We argue that the quality of initial conditions for decadal predictions should not purely be assessed by their closeness to observations, but also by the closeness of their respective predictions to observations. This prediction quality may depend on the representation of the simulated large-scale atmosphere–ocean feedback.

This article is categorized under:
Climate Models and Modeling > Knowledge Generation with Models

KEYWORDS

coupled data assimilation, decadal climate prediction, earth system model, large-scale atmosphere-ocean feedback, model-consistent initialization

1 | INTRODUCTION

In the past decade, efforts were made to predict Earth's climate on interannual to decadal time scales with advanced global coupled Earth System Models (ESMs) (Boer et al., 2016; Keenlyside & Ba, 2010; Marotzke et al., 2016;

Meehl et al., 2014; Smith et al., 2007, and references therein). For these predictions the ESM is initialized close to the observed state of the climate system at a certain point in time. This initial information is transferred by the ESM into the future by a proper representation of slow processes carrying memory on decadal time scales (e.g., storage and transport of heat in the ocean). During the prediction, the ESM is typically forced by prescribed external boundary conditions impacting Earth's radiative budget, such as solar irradiance, greenhouse gas concentration, stratospheric ozone and aerosol concentration, and major volcanic eruptions (Branstator & Teng, 2012; Cox & Stephenson, 2007). Eventually the quality of the predictions is measured by comparing predicted and observed parameters, provided that the observation period is long enough, for example for surface temperature and surface pressure fields. Despite ongoing improvements in terms of model physics and resolution, today's ESMs are only imperfect representations of the real world (Box 1). Therefore the question remains, how close to observations such an ESM could be initialized without introducing inconsistencies between the real world and the imperfect model world that would diminish the prediction quality.

A fundamental process responsible for the memory on interannual to decadal timescales is the interaction between atmosphere and ocean (Bjerknes, 1964). The large-scale atmosphere–ocean interaction in Earth's climate can be separated using different time scales. On shorter than interannual time scales, the ocean is forced by the atmosphere via heat and momentum fluxes as well as freshwater fluxes and gas exchanges at the atmosphere–ocean boundary (short-term atmosphere–ocean impact). High-frequency atmospheric variability is converted into low-frequency oceanic variability (Griffies & Bryan, 1997; Hasselmann, 1976; Latif & Barnett, 1994). On these time scales, the actual air-sea feedback at the atmosphere–ocean boundary in the Atlantic and extra-tropical Indo-Pacific ocean is negative throughout the year (Frankignoul et al., 2004; Frankignoul, Czaja, & L'Heveder, 1998), that is, the heat flux across the atmosphere–ocean boundary is damped. On interannual to decadal to centennial time scales, oceanic transports such as the circumglobal oceanic overturning circulation (Broecker, 1997; Stommel, 1958) facilitate global scale teleconnections. On these time scales, the variability of the atmosphere on a global scale is determined, albeit not exclusively, by the low-frequency oceanic variability (long-term ocean–atmosphere impact). Prominent examples for the large-scale atmosphere–ocean feedback on these time scales are the Atlantic multidecadal variability (AMV, Delworth, Manabe, & Stouffer, 1993) and the Pacific decadal oscillation (Mantua, Hare, Zhang, Wallace, & Francis, 1997).

BOX 1 CLIMATE SIMULATIONS—A BROADER PICTURE

Today's ESMs are aiming to comprehensively simulate Earth's climate. These simulations may obviously benefit from improvement to the ESM itself by, among others, incorporating any improved knowledge of physical processes into the ESM or improving the representation of interactions across scales and domains. A worldwide effort is represented by Phase 6 of the Coupled Model Intercomparison Project (CMIP6, Eyring et al., 2016). Starting with the pioneering work of Manabe and Bryan (1969), different components of the Earth's climate are traditionally separately represented in full-fledged ESMs, which may comprise of submodels for atmosphere, ocean, sea ice, land processes, and others, which are coupled together at certain times to exchange fluxes. Limitations in the knowledge of nature and its representation in an ESM as well as in the computational resources will always lead to imperfect simulations of Earth's climate by ESMs. Moreover, Earth's climate itself is only partly sampled by observations, and thus remains only imperfectly known.

Therefore, improved climate simulations may also result from more comprehensive observations of Earth's climate state that is by decreasing uncertainty in the reference the climate simulation is compared with, and by better capturing Earth's climate state for the initialization of climate predictions. Increasing the quality of observations is equally important than simply increasing the quantity of observations. In fact, climate simulations with an ESM could be used to determine key parameters, for example, large-scale oceanic transports, sea ice characteristics, or atmospheric processes, which could or should be observed or directly derived from observations in the future. Last but not least, due to the imperfection of both ESM and observations the incorporation (assimilation) of observations into an ESM asks for a model-consistent approach, which is honoring both the preferred model climate and the observed climate. Furthermore, the consistency needed in the assimilation depends on key interactions identified in nature, for example, the large-scale atmosphere–ocean feedback or the ice-atmosphere feedback, and should cover as many as necessary scales and submodels in an ESM.

The North Atlantic is an example of such a region with an important large-scale atmosphere–ocean feedback on decadal time scales (Hazeleger et al., 2013; Yeager & Robson, 2017, and references therein), which gives rise to enhanced interannual to decadal predictability of the North Atlantic ocean and adjacent continents (Borchert, Müller, & Baehr, 2018). The feedback is closely related to the AMV found in surface temperatures (Schlesinger & Ramankutty, 1994). The processes underlying this variability (Delworth et al., 1993; Grötzner, Latif, Timmermann, & Voss, 1999; Keenlyside, Latif, Jungclaus, Kornblueh, & Roeckner, 2008) are connecting the large-scale circulation of the atmosphere in the polar and subpolar North Atlantic with the oceanic subpolar gyre (SPG) and deep convection zones (Escudier, Mignot, & Swingedouw, 2013; Menary, Hodson, Robson, Sutton, & Wood, 2015; Robson, Ortega, & Sutton, 2016; Robson, Sutton, Lohmann, Smith, & Palmer, 2012). This in turn controls the strength and variability of the Atlantic meridional overturning circulation (AMOC) in the ocean and determines large parts of the multidecadal AMOC variability (Müller et al., 2015; Pohlmann et al., 2013; Robson et al., 2016; Srokosz et al., 2012). The AMOC realizes large parts of the northward heat transport from the subtropical to the subpolar latitudes (e.g., Buckley & Marshall, 2016), controlling the variability and the potential predictability of North Atlantic upper ocean heat content and surface temperatures on interannual to multidecadal time scales (Collins & Sinha, 2003; Pohlmann et al., 2004).

In this context, the relation of AMOC strength and SPG strength is an important question. Experiments with coupled climate models suggest that the decadal AMOC variability is out of phase, if not anticorrelated, with the strength of the SPG: Zhang (2008) found the AMOC strength to be anticorrelated with SPG sea surface height and SPG strength, Robson et al. (2016) showed that the warming and weakening of the SPG in the mid 1990s was associated by an increase in AMOC strength. It has been recently discussed (Clement et al., 2015, 2016; Gulev, Latif, Keenlyside, Park, & Koltermann, 2013; McCarthy, Joyce, & Josey, 2018; Zhang et al., 2016), how the variability in heat exchange between ocean and atmosphere on these time scales could be responsible for changes in the variability of the large-scale circulation of the atmosphere. In a recent study, Wills, Armour, Battisti, and Hartmann (2019) found that a dynamical coupling of oceanic and atmospheric circulation, closing the two-way large-scale atmosphere–ocean feedback, is necessary to explain the AMV as a coupled atmosphere–ocean process. A consistent interaction of atmospheric and oceanic components may therefore be mandatory in any ESM to be used for interannual to decadal climate prediction.

The ESMs used in interannual to decadal prediction are designed to simulate a stable climatology close to the observed one over decades to centuries. In these model simulations, the large-scale atmosphere–ocean interaction is generally well represented and the internal variability is in a statistical sense close to the observed one (intergovernmental panel on climate change fifth assessment report, Flato et al., 2013; Wills et al., 2019). In "historical" experiments, an ESM can be used to simulate Earth's climate under the observed global warming history from 1850 onward incorporating changes in the external radiative forcing, which are mainly due to anthropogenic emissions of greenhouse gases (Eyring et al., 2016). The historical simulation is not constrained by observations of the state of atmosphere and ocean, except for greenhouse gas concentration and volcanic aerosols. Climate predictions with an ESM on interannual to decadal time scales should therefore additionally benefit from observations of the thermodynamic state of Earth's climate (Doblas-Reyes et al., 2013; Pohlmann, Jungclaus, Köhl, Stammer, & Marotzke, 2009; Polkova, Köhl, & Stammer, 2014; Smith et al., 2007, among many others). The simultaneous incorporation of observations from atmosphere and ocean, known as "coupled data assimilation" (Penny et al., 2017), initializes the ESM with the correct timing of the variability on these time scales, in contrast to the uninitialized historical simulation. However, observations do not fully sample the state of the Earth's climate system. Especially the state of the subsurface ocean remains largely unobserved, let alone large overturning circulations like the AMOC. In such an undersampled oceanic system, the atmosphere–ocean impact related to the assimilation of atmospheric observations into the atmospheric component of an ESM could be successfully used to constrain the oceanic component in that ESM as well.

In coupled data assimilation, advanced numerical methods, such as the ensemble Kalman filter (EnKF, Evensen, 1994) have been introduced to incorporate observations into the ESM. The EnKF can be adapted to almost any ESM (Anderson et al., 2009; Nerger & Hiller, 2013) and has been increasingly used in recent years in a weakly coupled framework to initialize interannual to decadal climate predictions (Brune, Düsterhus, Pohlmann, Müller, & Baehr, 2018; Counillon et al., 2014; Karspeck, Yeager, Danabasoglu, & Teng, 2015; Msadek et al., 2014). Moreover, the EnKF could potentially operate across model domains facilitating strongly coupled assimilation (Penny et al., 2017; Sluka, Penny, Kalnay, & Miyoshi, 2016). Theoretically, the assimilated model state could track the observed state in a way that represents both the model dynamics and the observations in an optimal way. Practically, this approach comes with the expensive use of computer resources, for example, the need of large ensemble simulations or iterative simulations. As a compromise, suboptimal solutions may be taken into account, that is, a smaller ensemble size for the EnKF combined with localization and artificial inflation (Houtekamer & Zhang, 2016). In contrast to the EnKF, the Newtonian

relaxation ("nudging", e.g., Hoke & Anthes, 1976; Lakshmivarahan & Lewis, 2013) of the state of the components of an ESM to reanalyses (García-Serrano, Guemas, & Doblas-Reyes, 2015; Kröger, Müller, & von Storch, 2012; Servonnat et al., 2015; Volpi, Guemas, & Doblas-Reyes, 2017) is low in demand of computer resources. However, nudging has to be used with caution. The empirical approach toward the nudging coefficients offers a simple way to subjectively fit the model state to the observed state (Lei & Hacker, 2015). Strong inconsistencies between model and observation may lead to unrealistic compensations within the model, for example, anomalous heat fluxes compensating for temperature biases (Servonnat et al., 2015). While nudging atmospheric and oceanic components of an ESM toward stand-alone atmospheric or oceanic reanalysis products, any imbalances between these reanalyses are directly imported into the ESM. In addition, the systematic inability of the model to digest the reanalysis may even lead to further imbalances. For example, in the North Atlantic model biases in the correct position of ocean gyres and the overturning circulation may lead to imbalances in the ocean heat budget (Kröger et al., 2018). With nudging, the potential large-scale atmosphere–ocean feedback emerging from the unrestricted ESM itself may be suppressed.

Here, we review how prediction quality of an ESM changes in relation to the closeness of the initializations to the free model state and to the observed state. The weakly coupled data assimilations used in these initializations all aim to honor both the free model state and the observed state, but to a different degree. Since we aim to predict the interannual to decadal time scales, the "fast" atmosphere–ocean impact during assimilation will not so much depend on how the atmospheric component is restricted to atmospheric observations, as long as it is restricted at all. We therefore nudge the atmospheric component to reanalyses in all of our experiments to take advantage of the low demand in resources of this method. The large-scale atmosphere–ocean feedback will then depend on how a consistent atmosphere–ocean impact is allowed by the way the oceanic component is restricted to oceanic observations. We present four experiments to illustrate the impact of different restrictions of the oceanic component with respect to observations. In a set of reforecasts ("hindcasts") for each of the four restrictions with the same ESM, we analyze the representation of strength and variability of the AMOC as a highly integrated oceanic parameter, albeit only observed since 2004 (Cunningham et al., 2007; Smeed et al., 2014), and, as complementarily, the predictability of the AMV and North Atlantic SPG sea surface temperatures (SSTs). Both have been observed for a much longer time period (Good, Martin, & Rayner, 2013; Rayner et al., 2003) than the AMOC. By incorporating a historical ensemble simulation into our analysis as a reference point, we aim to establish the role of the atmosphere–ocean impact as well as the role of an initialization close to observations.

2 | LARGE-SCALE ATMOSPHERE–OCEAN FEEDBACK IN INITIALIZATION OF CLIMATE PREDICTIONS

We use a suite of prediction experiments performed with the Max Planck Institute Earth System Model (low resolution, MPI-ESM-LR) with spectral resolution T63 and 47 levels in the atmospheric component and nominal 1.5° horizontal resolution and 40 levels in the oceanic component (Giorgetta et al., 2013). All assimilations and a 10-member historical ensemble simulation are started from a preindustrial control simulation with MPI-ESM-LR, they use Phase 5 of the Coupled Model Intercomparison Project (CMIP5) external forcing (Taylor, Stouffer, & Meehl, 2012). The experiments differ in the way they allow for a consistent oceanic response to the atmospheric nudging (simple relaxation to a reference field) during the assimilation phase (Table 1). We investigate several assimilation possibilities between two extreme cases: oceanic observations are not assimilated into the ESM at all (nudgAf), allowing for a full atmosphere–ocean impact within the assimilation experiment, or the oceanic component of MPI-ESM-LR is fully nudged to oceanic reanalysis data (nudgOf), largely suppressing the atmosphere–ocean impact within the assimilation experiment. Vice versa, the greater part of the ocean–atmosphere impact within the assimilation experiment is suppressed by the atmospheric nudging in all experiments. Our four assimilation experiments use the same assimilation method for the atmospheric component: spectral full-value nudging to ERA40/ERAInterim atmospheric reanalyses (Dee et al., 2011; Uppala et al., 2005) from ECMWF, but distinctly different methods for the oceanic component (Table 1): (1) no assimilation of oceanic observations resulting in an oceanic initialization relying on atmospheric nudging with full atmosphere–ocean impact; (2) once-a-month assimilation of full-value temperature and salinity observations (profiles from EN4, Good et al., 2013) with a 16-member EnKF (Brune et al., 2018; Brune, Nerger, & Baehr, 2015; Polkova et al., 2019), oceanic initialization depends on oceanic observations only within the EN4-observed grid cells and only at the EnKF analysis time step at the beginning of each month, everywhere else and at every other time step oceanic initialization relies on the impact of the atmospheric nudging; (3) continuous full-grid anomaly nudging (Pohlmann et al., 2013) to monthly

TABLE 1 Family of coupled data assimilations to initialize interannual to decadal predictions with Max Planck Institute Earth System Model (low resolution, MPI-ESM-LR)

	Historical	nudgAf	enkfOf	nudgOa	nudgOf
Atmospheric assimilation	None	Continuous full-value spectral nudging divergence, vorticity, temperature, and sea level pressure from ERA40/ERAInterim reanalyses			
Oceanic assimilation	None	None	Full-value 16-member ensemble Kalman filter (EnKF) with once-a-month T,S profiles from EN4	Anomaly Continuous full-grid nudging to T,S from ORAS4 reanalysis	Full-value
Large-scale feedback in assimilation	Full impacts atmosphere–ocean ocean–atmosphere	Full impact atmosphere–ocean	Partly realized impact atmosphere–ocean Outside T,S observations or between updates	Mean state respected	Almost no feedback

Notes: All simulations are driven by the similar external forcing (Phase 5 of the Coupled Model Intercomparison Project, CMIP5, Taylor et al., 2012). The historical ensemble does not incorporate any observations of the climate state and serves as the uninitialized experiment to compare against. All four assimilations use the same method in the atmospheric component but differ in the method used in the oceanic component. Atmospheric and oceanic assimilations interact with each other only via the coupling of the atmospheric and oceanic components of the Earth System Models (ESM) (weakly coupled assimilation). Every simulation stands for a different realization of the large-scale atmosphere–ocean feedback during the assimilation phase. Hindcasts are performed with a 10-member ensemble initialized from the respective assimilation. The reanalyses are taken from the ECMWF, for the atmosphere ERA40/ERAInterim (Dee et al., 2011; Uppala et al., 2005), and for the ocean ORAS4 (Balmaseda, Mogensen, & Weaver, 2013). Oceanic temperature and salinity (T,S) profiles are taken from EN4 (Good et al., 2013).

temperatures and salinities from ORAS4 oceanic reanalysis (Balmaseda et al., 2013) from ECMWF, the model mean bias is kept unchanged at every grid cell, the oceanic initialization depends strongly on ORAS4 and only weakly on the atmospheric nudging, the atmosphere–ocean impact is low; and (4) continuous full-grid full-value nudging (Kröger et al., 2018; Marotzke et al., 2016) to monthly temperatures and salinities from ORAS4 prohibiting any atmosphere–ocean impact on the oceanic initialization. The systems (3) and (4) were also part in the heat budget analysis of Kröger et al. (2018), as "ORAS4-ANOM" and "ORAS4-FULL," respectively.

A set of retrospective ensemble predictions (hereafter: hindcasts) with 10 members is initialized from each of the four assimilation experiments. All predictions are only restricted by external forcing and allow for a full large-scale atmosphere–ocean feedback. Out of the ensemble generation methods tested for decadal predictions with MPI-ESM-LR (Marini, Polkova, Köhl, & Stammer, 2016; Polkova et al., 2019; Romanova & Hense, 2017) we use two, the EnKF implicit to the EnKF system, and 1-day-lagged initialization for the other three systems. For each prediction system, ensemble hindcasts are initialized from the respective assimilation on November 1 in every year from 1960 to 2013, running for 10 years and 2 months, respectively. In addition, we analyze an uninitialized prediction based on an ensemble of historical simulations with MPI-ESM-LR, providing the full large-scale atmosphere–ocean feedback as well, but completely lacking the impact of observations.

All assimilations are started from a comprehensive and several hundred years long free model simulation of MPI-ESM-LR with preindustrial external forcing conditions. Thus, at the start of the assimilations, the large-scale atmosphere–ocean feedback is consistent within the model world, but not necessarily fully consistent with the real world (Frankignoul et al., 1998, 2004). Our hindcasts are free model simulations only restricted by real external forcing conditions. They take advantage of the model-consistent large-scale atmosphere–ocean feedback they inherit from the preindustrial control simulation with MPI-ESM-LR.

While incorporating observations during assimilation, we try to reconcile the model climate and the past observed climate with the aim to initialize predictions of the future observed climate. We therefore measure the quality of our prediction systems rather by the quality of the predictions with respect to the future observed climate than by the quality of the assimilation with respect to the past observed climate.

3 | REPRESENTATION OF OVERTURNING CIRCULATION

One of the key processes describing the North Atlantic climate is the AMOC (Box 2). In the North Atlantic large-scale atmosphere–ocean feedback, the AMOC is responsible for the transport of oceanic properties such as heat and salinity from the subtropical to the subpolar latitudes (Buckley & Marshall, 2016; Delworth et al., 1993). The AMOC integrates

BOX 2 ATLANTIC MERIDIONAL OVERTURNING CIRCULATION

As a part of a system of large-scale oceanic circulations circumnavigating the globe and realizing the large-scale ocean heat transport, the AMOC consists of two branches (Buckley & Marshall, 2016). The near surface branch transports warm and saline waters from the tropical Atlantic into the North Atlantic mid-latitudes and polar latitudes and thus contributes to the rather mild climate in North-western Europe. The deep branch transports cold water back to the South and is connected to the surface branch via deep convection zones in the Labrador, Irminger, and Nordic Seas, where atmospheric cooling leads to the formation of cold dense waters.

Continuous direct observations of the AMOC exist with the dedicated RAPID-MOCHA array at 26.5°N, but not before 2004 (Cunningham et al., 2007; Kanzow et al., 2007; Smeed et al., 2014). Further studies tried to derive AMOC strengths indirectly, for instance from temperature and salinity profiles measured by Argo floats and altimeter observations (Willis, 2010). Thus a large uncertainty remains when describing the AMOC evolution over the last century. Nevertheless, the importance of the AMOC in particular for the North Atlantic climate (Griffies & Bryan, 1997) calls for special attention to be paid in climate models on the representation of the AMOC (Flato et al., 2013). Since the AMOC is a highly integrated quantity, that is sensitive to many factors across a wide range of spatiotemporal scales in both atmosphere and ocean, the AMOC can be used to assess the usability of models and simulations in the context of climate prediction, even without a proper observational reference.

For the initialization of decadal predictions, the AMOC is typically not directly assimilated, but is rather indirectly simulated by the assimilation of better observed quantities, such as oceanic temperatures and salinities, sea surface heights, and atmospheric wind fields. The AMOC may be very sensitive to the assimilation method (Baehr, 2010). Using the entire oceanic observational database with different assimilation schemes may lead to different AMOC realizations in the same global coupled climate model (Karspeck et al., 2017), rendering the simulation of the AMOC on interannual to decadal time scales a demanding task.

atmospheric and oceanic drivers over a large range of temporal and spatial time scales and thus represents a part of the memory of the climate system on interannual to decadal time scales. We take the AMOC as a proxy for this memory and analyze how our initializations impact the AMOC mean cell and its variability in time. Since observations of the full AMOC cell do not exist, we focus on the differences between the initialized simulations as well as in the comparison with the historical ensemble and the ORAS4 reanalysis data.

In an earlier study, Tardif, Hakim, and Snyder (2015) showed in a perfect low-order coupled atmosphere–ocean data assimilation framework that the reconstruction of the low-frequency variability of the AMOC, that is, decadal time scales and longer, benefits from low-frequency oceanic observations but not from high-frequency atmospheric observations. However, AMOC variability on decadal time scales may be connected to low-frequency atmospheric variability like the North Atlantic Oscillation (Danabasoglu et al., 2016; Ortega, Hawkins, & Sutton, 2011), and would thus benefit from the assimilation of low-frequency atmospheric observations as well.

We therefore expect a dependence of the AMOC cell (time mean in Figure 1, standard deviation in Figure 2) on the oceanic assimilation method that we use in addition to the atmospheric nudging.

The structure and strength of the AMOC mean cell is not substantially changed by atmospheric nudging alone in comparison to the uninitialized historical ensemble, but oceanic assimilation may do so (left column in Figure 1). The oceanic EnKF assimilation changes the time mean AMOC cell considerably by deepening the upper circulation cell and thereby shrinking the lower circulation cell, the observed oceanic temperature and salinity profiles have a strong impact. Anomaly nudging leads by design to a time mean AMOC cell similar to the historical ensemble, because it uses the time mean oceanic temperatures and salinities from the historical ensemble to calculate the nudging term. Full-value nudging by design strongly drags the ocean state to the ORAS4 reanalysis data, the simulated time mean AMOC cell is thus very similar to that from the reanalysis. In this way, rather unrealistic subcells emerge (Figure 1h), similar to the findings of Smith et al. (2013), Karspeck et al. (2017), and Kröger et al. (2018).

The mean AMOC cell from assimilation is important for the predicted AMOC cell because in all simulations, the overall structure of the time mean AMOC cell from the initialization is retained at least until lead year 5 (Figure 1, right column). The pattern correlation of the initialized AMOC time mean cells with the uninitialized simulation hardly

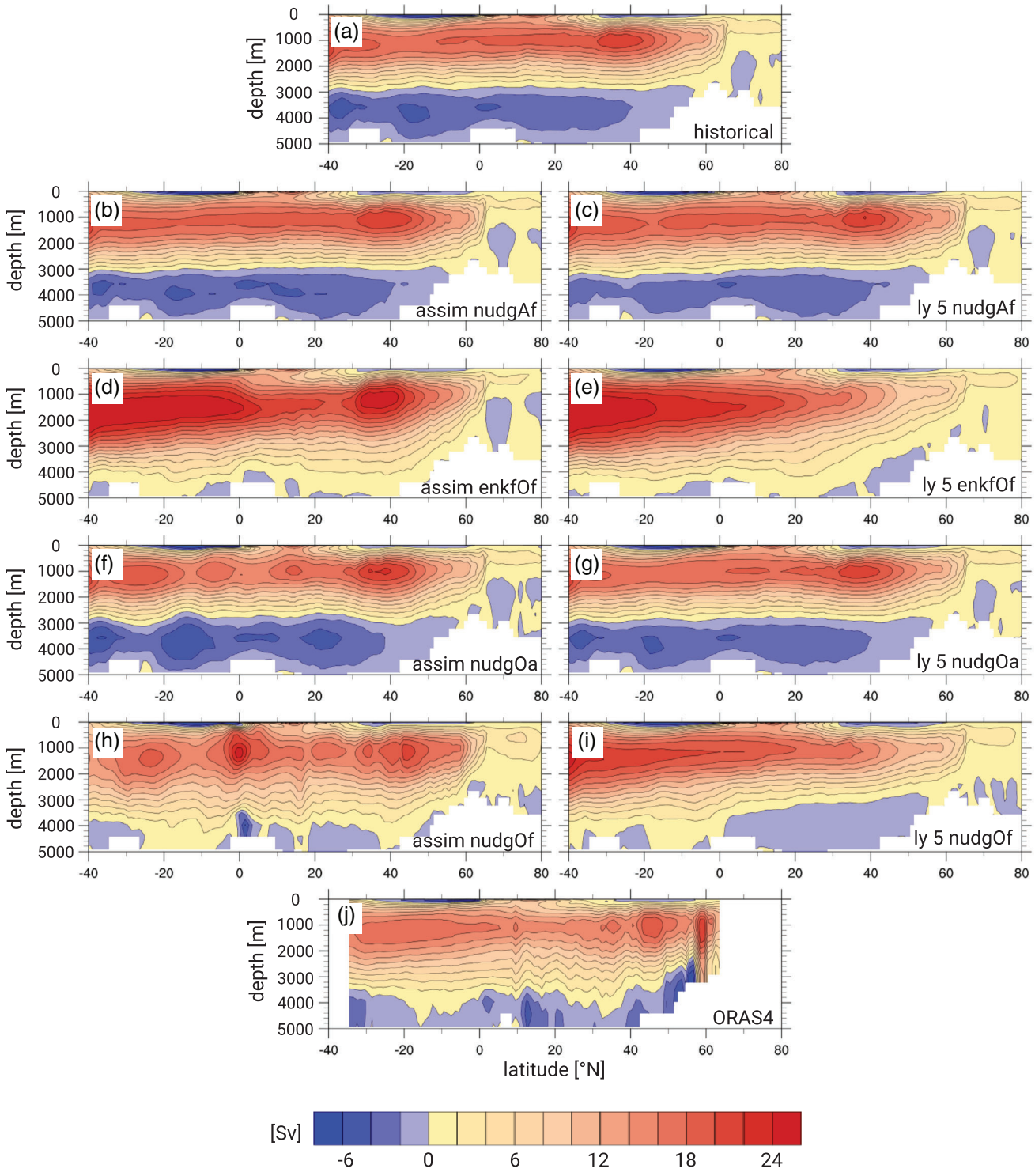

FIGURE 1 The time mean (1961–2013) Atlantic meridional overturning circulation (AMOC) cell depends on the assimilation method (left column, see also Smith, Eade, & Pohlmann, 2013). The hindcasts inherit the general pattern of their AMOC mean cell from the assimilation for lead year all lead years (lead year 5 shown in the right column). The oceanic assimilation method determines how close the mean cell is to either the uninitialized historical ensemble (upper panel) or the ORAS4 reanalysis data (lower panel) used during assimilation. With atmospheric nudging only (nudgAf), the mean cell is very close to the historical ensemble with a distinct clockwise circulation above 3,000 m depth and a anticlockwise circulation below (b,c). A similar mean cell is simulated when additionally the ocean is anomaly nudged (nudgOa) toward reanalysis data (f,g). The ensemble Kalman filter (EnKF) assimilation of full-value observed oceanic profiles (enkfOf) changes the mean cell significantly (d), these changes also persist in lead year 5 (e). The full-value nudging toward reanalysis data (nudgOf) effectively imprints large- and small-scale features of the mean cell of ORAS4 onto Max Planck Institute Earth System Model (low resolution, MPI-ESM-LR) during assimilation (h) and the large-scale features still persist in lead year 5 (i). The lead year dependency of the pattern correlation of the initialized AMOC mean cells with the uninitialized AMOC mean cell is shown in Figure 3

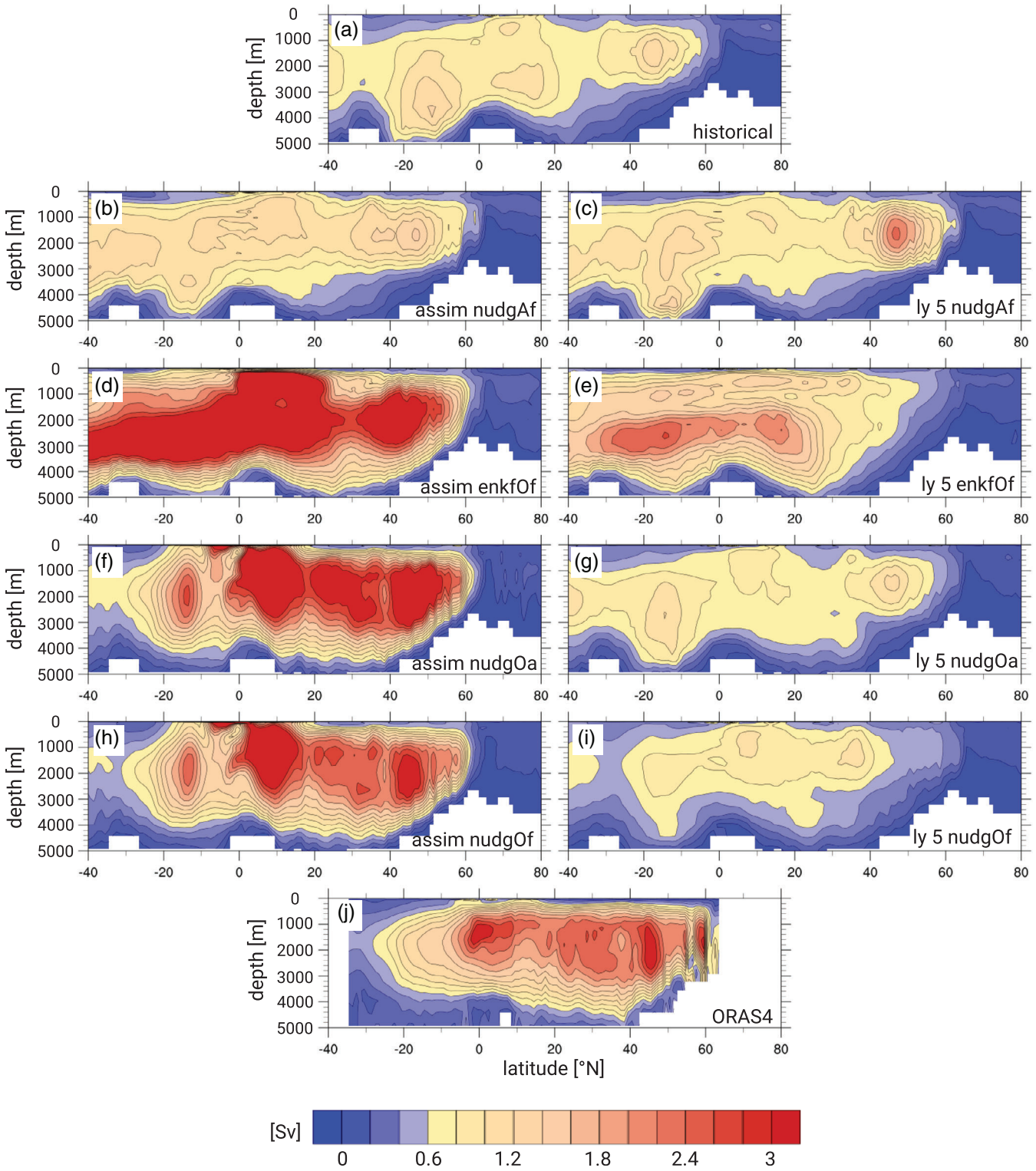

FIGURE 2 The year-to-year variability (1961–2013) of the Atlantic meridional overturning circulation (AMOC) cell in terms of the ensemble mean of the standard deviation of yearly mean values depends on the assimilation method (left column), but this dependence persists only in the first lead years and is hardly visible in lead year 5 (right column). The atmospheric assimilation alone (nudgAf, b, c) accounts only for a minor part in changes when compared to the historical ensemble (upper panel). The major part of these changes comes from the oceanic assimilation. Here, both anomaly nudging (nudgOa, f) and full-value nudging (nudgOf, h) to ORAS4 reanalysis data results in a transfer of the variability of the re-analysis (lower panel) to the Max Planck Institute Earth System Model (low resolution, MPI-ESM-LR). Oceanic ensemble Kalman filter (EnKF) assimilation of observed T and S profiles (enkfOf, d) shows a similar strong variability. In all hindcast simulations, the variability becomes similar to that from the uninitialized historical ensemble from lead year 5 onward. The lead year dependency of the pattern correlation of the variability of the initialized AMOC cell with that of the uninitialized AMOC cell is shown in Figure 3

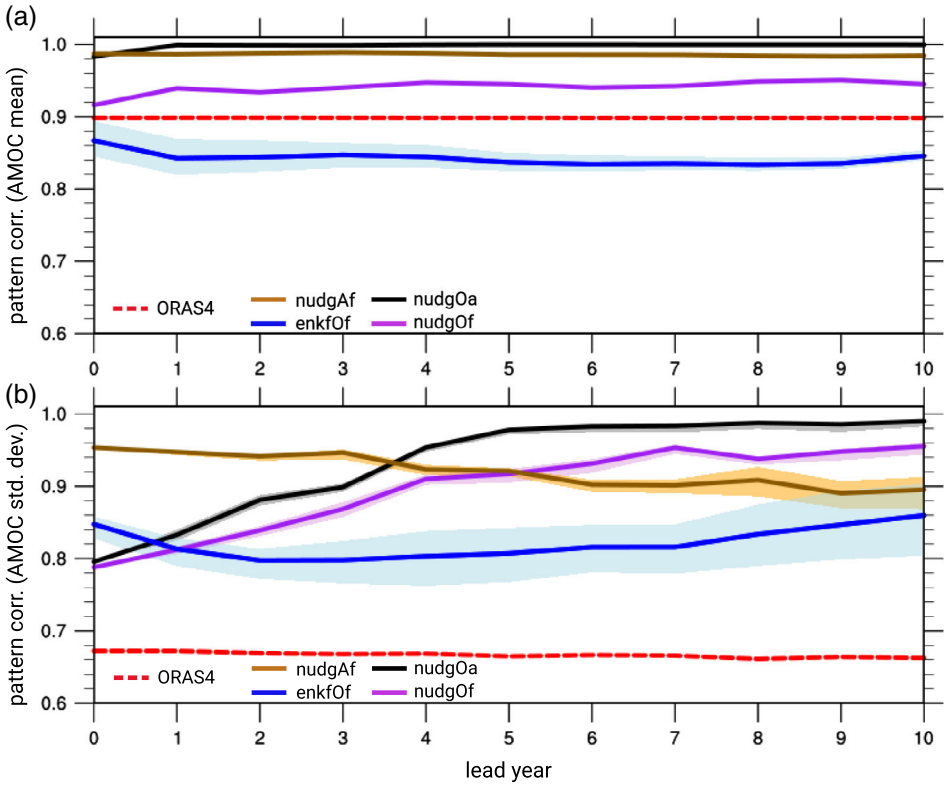

FIGURE 3 The pattern correlation of the initialized Atlantic meridional overturning circulation (AMOC) cell (mean and year-to-year variability) with that of the uninitialized historical ensemble (Figures 1 and 2, respectively) is a measure of similarity between the initialized and uninitialized simulations. (a) The pattern correlation for the AMOC mean cells depends on the assimilation method, changes over lead time are small and the differences are maintained over all lead times. (b) The pattern correlation for the year-to-year variability also depends on the assimilation method, but it changes over lead time. The two systems applying oceanic nudging have a lower correlation with the uninitialized system during assimilation than the other two systems, but not as low as the ORAS4 reanalysis. Both nudging systems show an increasing correlation and therefore similarity with the uninitialized system after assimilation with some saturation after lead year 5. The impact of the oceanic ensemble Kalman filter (EnKF) assimilation lasts longer, the correlation increases only after lead year 3 as does the uncertainty, and does not reach a saturation before lead year 10. For the system with atmospheric nudging only, correlation is high during assimilation and the first five lead years. It slightly drops off toward lead year 10 with increasing uncertainty

changes over the first 10 lead years (Figure 3a), the time scale for changes in the AMOC mean cell maybe much longer (Persechino et al., 2012, their Figure 1a). Thus, in all simulations, the mean AMOC cell carries memory on the inter-annual to decadal time scale.

The year-to-year variability of the AMOC cell, expressed as its standard deviation, also depends on the assimilation method (Figure 2). All our assimilation experiments lead to an increased AMOC variability in comparison to the ensemble mean of the historical ensemble (left column in Figure 2). Atmospheric nudging alone only accounts for a minor part of this increase, while all oceanic assimilation methods have a strong impact, which corroborates the findings of Tardif et al. (2015). The oceanic EnKF assimilation leads to the highest variability of all assimilation systems. Both anomaly and full-value nudging imprint the year-to-year variability of the ORAS4 reanalysis data on MPI-ESM. In contrast to the time mean AMOC cell, the effect of assimilation on the predicted AMOC year-to-year variability changes with lead time depending on the initialization method (lead year 5 in right column in Figure 2). With increasing lead time, the variability of both initializations incorporating ORAS4 by nudging becomes more similar to that of the uninitialized simulation, the pattern correlation increases (Figure 3b). This effectively sets a 5-year limit to the potential predictability of the AMOC due to initialization via ORAS4 nudging, similar to the findings of Tiedje and Baehr (2014). In the two other systems, there is not such a sharp limit, the year-to-year variability is still different from the uninitialized simulation in the later lead years (Figure 3b). We further investigate if this could give rise to an extended prediction horizon in the next section.

4 | PREDICTABILITY OF OVERTURNING CIRCULATION

Even though observations for the full AMOC cell are not available, the AMOC has been continuously observed at several latitudes, most notably at 26.5°N (RAPID-MOCHA array, Cunningham et al., 2007; Kanzow et al., 2007; Smeed et al., 2014) from 2004 onward. At this latitude, earlier studies (Matei et al., 2012; Müller et al., 2017) already found predictability in the interannual variability since 2004.

The simulated AMOC time series at 26.5°N from 1961 to 2013 during assimilation (Figure 4a) is largely determined both by multidecadal changes in the mean state in relation to the AMV and by interannual variability. The impact of the assimilation method is different for the interannual and the decadal variability of the AMOC. Atmospheric nudging to reanalysis data controls the interannual variability in all assimilations. Although such prescribed atmospheric conditions may also exert control on the decadal variability of the AMOC (Danabasoglu et al., 2016; Ortega et al., 2011), the oceanic assimilation methods ultimately control the differences in decadal variability between our prediction systems: oceanic nudging to reanalysis data results in an AMOC very similar to that of ORAS4 during assimilation and oceanic EnKF leads to an AMOC with a decadal variability which differs from all our other simulations. While these differences in variability are retained by the initialized hindcasts with decreasing strength over the first five lead years (Figure 4b), similarities of the predicted AMOC with that from the historical ensemble are growing with lead time.

We further illuminate this by analyzing the probability distribution of the AMOC around 26.5°N. Here, our focus lies for each prediction system on both shape and mean of the cumulated distribution over all ensemble members (Figure 5) in comparison with the distribution from the uninitialized historical ensemble, which shows a narrow and almost Gaussian shape around a mean transport of 18.5 Sv, and the reanalysis' distribution with a wide and double peaked shape around a mean of 15 Sv.

With atmospheric nudging only, the AMOC around 26.5°N is already initialized with a shape close to the historical ensemble with slightly more weight on the large transports (Figure 5a). Nudging of the ocean toward reanalysis data essentially reshapes the distribution to that from re-analysis, though shifted to larger transports. For the anomaly

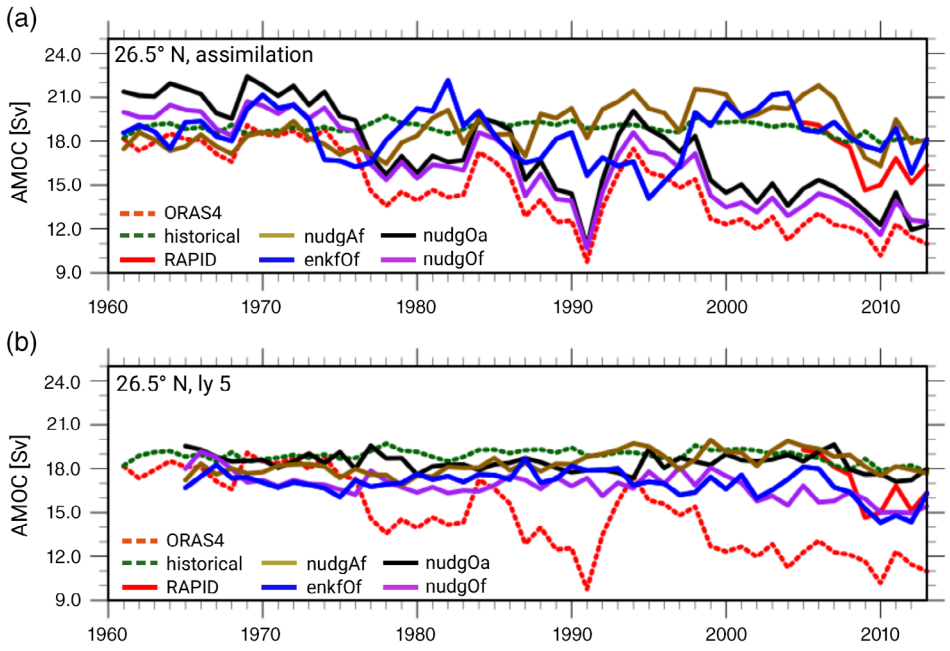

FIGURE 4 (a) In the time series of the simulated ensemble mean Atlantic meridional overturning circulation (AMOC) at 26.5°N during assimilation, interannual variability is dominant when only the atmosphere is nudged (nudgAf, brown). Multidecadal variability is introduced by oceanic assimilations. Here, both anomaly nudging (nudgOa, black) and full-value nudging (nudgOf, purple) lead to a similar AMOC evolution than in the ORAS4 reanalysis data (dashed red), even down to the abnormally low AMOC in 1991. Oceanic ensemble Kalman filter (EnKF) assimilation (enkfOf, blue) results in an AMOC evolution different to any of other simulations before the 2000s. However, for the period after 2004, the observations from RAPID-MOCHA (solid red, Smeed et al., 2014) are, except for a mean offset, met by all assimilations. The impact of assimilation decreases over the lead years. (b) In the lead year 5, time series of the simulated ensemble mean AMOC at 26.5°N, the variability is not much different any more from the uninitialized historical ensemble (dashed green)

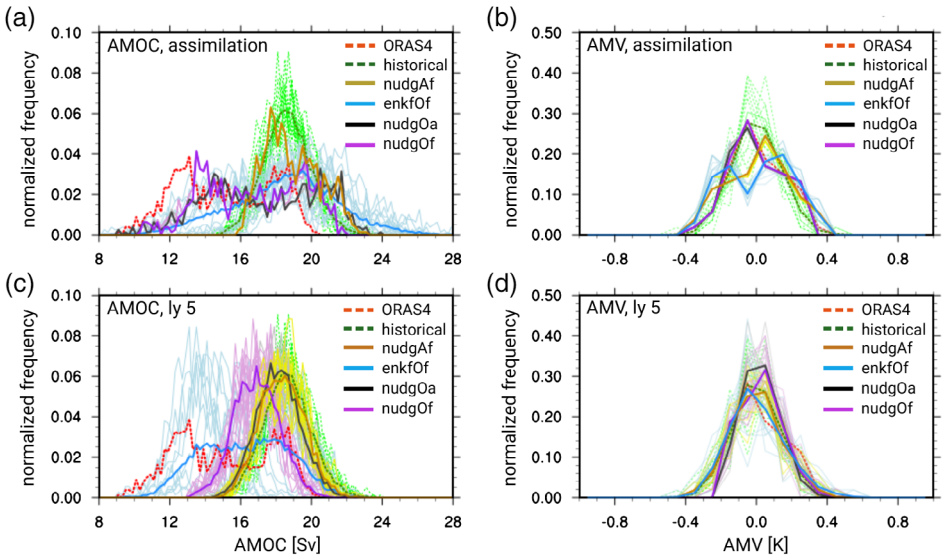

FIGURE 5 The probability distribution of Atlantic meridional overturning circulation (AMOC) between 24 and 28 °N (a,c) and of the Atlantic multidecadal variability (AMV) (b,d) for the time period 1961–2013. (a) The AMOC distribution during assimilation depends on the assimilation method. Atmospheric nudging only (nudgAf, brown) leads to a narrow distribution similar to the historical ensemble (dashed green), all oceanic assimilations lead to a much wider distribution more similar to ORAS4 reanalysis data (dashed red). Both anomaly nudging (nudgOa, black) and full-value nudging (nudgOf, purple) resemble the double-peak distribution from reanalysis data, whereas oceanic ensemble Kalman filter (EnKF) assimilation (enkfOf, blue) results in a one-peak distribution. (c) In lead year 5, the shapes of the distributions become more similar to the historical ensemble in all hindcasts with some offset in the mean, the largest difference to the historical ensemble remains with the EnKF system. (b) The distribution of the AMV during assimilation only partly depends on the assimilation method (b), with the some differences due to oceanic EnKF assimilation and oceanic full-value nudging. (d) In lead year 5, the AMV distributions are similar in all simulations. Please note that thick lines represent the cumulated distributions over all 10-ensemble members, thin lines distributions for each of the 10-ensemble members, respectively

nudging the mean transport is 17 Sv, the offset to the reanalysis is related to the mean oceanic state taken from the historical ensemble in the nudging process. Also, since the AMOC is not directly nudged, an additional offset can be seen due to the integrating effect of the AMOC even in the full-value oceanic nudging with a mean transport of 16.5 Sv. The oceanic EnKF assimilation alters the distribution to a wide single-peaked shape, but with a mean transport (18.5 Sv) close to that of the uninitialized historical ensemble. In lead year 5 (Figure 5b), the shapes of the AMOC distributions of all initialized hindcasts are all single peaked and closer to that from the historical ensemble than to that from reanalysis. The mean transports are close to the uninitialized historical ensemble as well. The most long lasting impact of initialization can be seen with the EnKF method.

Impacts of the oceanic assimilation method on the AMOC at 26.5°N are similar to those on the whole AMOC cell, we therefore calculate the AMOC prediction skill of our simulations in terms of the lead year dependent correlation of the simulated AMOC at 26.5°N over the period 2004–2013 (Figure 6, cf. Matei et al., 2012; Müller et al., 2017). A cautious interpretation of the results is necessary due to the still rather short time period of observations. Nevertheless, we will combine the AMOC prediction skill as a measure of the oceanic circulation with the AMV prediction skill as a measure of the large-scale coupled atmosphere–ocean feedback in the next chapter.

Hindcasts initialized by atmospheric nudging only or with additional oceanic EnKF assimilation lead to larger correlation skill with RAPID-MOCHA than the historical ensemble in lead years 1 to 5. For the systems using nudging to reanalysis data the low correlations in lead years 1 to 5 point to a systematic mistiming of the year-to-year variability with a strong initialization shock in the first lead year. The lower than historical correlations for almost all hindcasts lead years after 5 show that these years are currently beyond the prediction horizon of any of our initialized prediction systems.

The oceanic assimilation method forces the model to a specific mean AMOC regime, which is broadly maintained throughout the whole hindcast period of 10 years. The assimilation method determines the allowed atmosphere–ocean impact and thus also determines how much of the mean AMOC cell simulated in the historical ensemble is retained: lesser atmospheric impact means larger deviation from the historical ensemble. Likewise the assimilation method

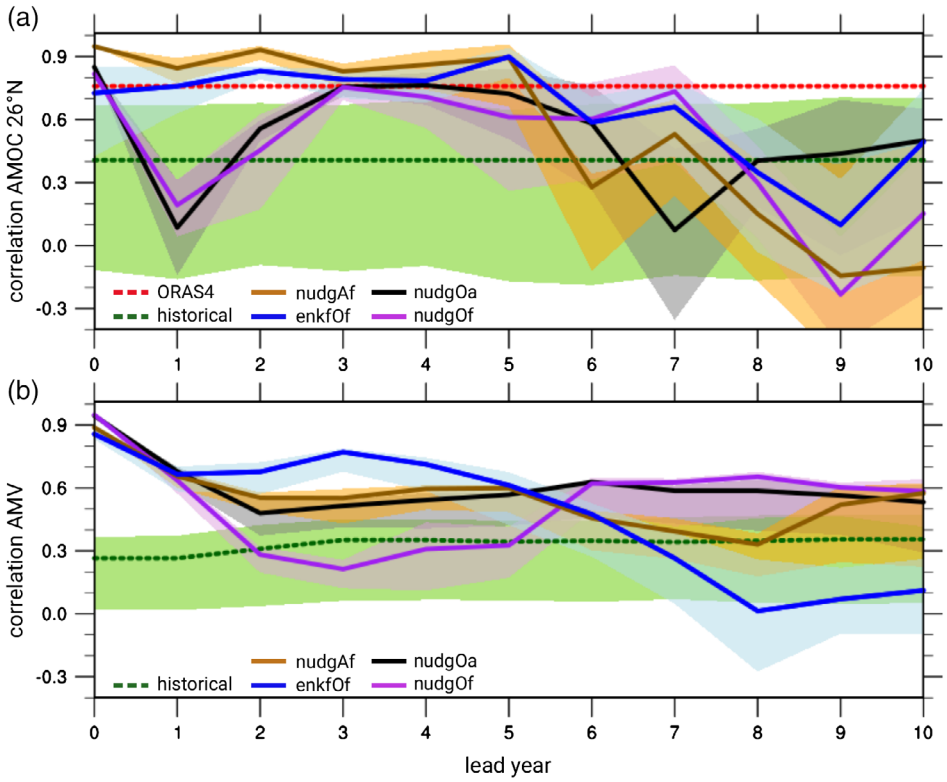

FIGURE 6 (a) The prediction skill of Atlantic meridional overturning circulation (AMOC) at 26.5°N in terms of correlation with RAPID-MOCHA observations (Smeed et al., 2014) over the period 2004–2013 is lead year dependent. Atmospheric nudging alone (nudgAf, brown) and the oceanic ensemble Kalman filter (EnKF) assimilation (enkfOf, blue) result in significantly higher prediction skill, that is, shaded areas do not overlap, than the uninitialized historical ensemble (dashed green) for lead years 1 to 5. Nudging to reanalysis data, either anomaly (nudgOa, black) or full-value (nudgOf, purple), results in a high correlation during assimilation but in low correlations in lead years 1 and 2, due to an initialization shock (Kröger et al., 2018). The prediction horizon for AMOC at 26.5°N with the Max Planck Institute Earth System Model (low resolution, MPI-ESM-LR) is at five lead years. After this time, skill does not significantly differ between the simulations. (b) The prediction skill of Atlantic multidecadal variability (AMV) in terms of correlation with HadISST (Rayner et al., 2003) is high for all initialized systems in lead year 1 but differs considerably from lead year 2 to 5. Here, the EnKF system outperforms all other systems while the system with oceanic full-value nudging is not better than the uninitialized historical ensemble. After lead year 5, the EnKF system looses its good prediction skill, and none of the initialized systems significantly outperforms the uninitialized historical ensemble. The prediction horizon for AMV is at lead year 5, similar to that for AMOC. Please note that the thick line represents the skill of the ensemble mean, the shaded areas indicate the spread in skill based on 95% of the bootstrapped ensemble mean

imprints a year-to-year variability, but this impact lasts longest for only 5 years. After lead year 5, variability is close to that from the historical ensemble, eventually setting a limit of about 5 years regarding any AMOC predictability with MPI-ESM-LR. That is corroborated by the drop in skill after lead year 5 we found at 26.5°N in all examined prediction systems.

5 | REPRESENTATION AND PREDICTABILITY OF AMV

We complement our AMOC analysis with an assessment of the AMV (Delworth et al., 1993). The AMV is calculated from large-scale North Atlantic SSTs, where observations exist longer than for AMOC. Similar to the AMOC, the AMV represents an integrating quantity within the coupled atmosphere–ocean system, thus the variability of AMV may benefit from a consistent large-scale atmosphere–ocean feedback. There remains some uncertainty in our AMV assessment, since we know that our analysis (1961–2013) does not fully cover a full AMV cycle of ≈70 years, and that the predictability of North Atlantic SSTs depends on the AMV phase (Borchert, Düsterhus, Brune, & Baehr, 2019; Brune et al., 2018).

The representation of the AMV during assimilation over the time period 1961–2013 (probability distribution in Figure 5b) depends only partly on the assimilation method. The oceanic EnKF assimilation and the oceanic full-value

nudging are leading to the largest, but still minor differences in the AMV variability. In lead year 5, the inability of the two systems with oceanic nudging to fully represent the negative tail of the AMV distribution (Figure 5d) is the only difference between the simulations. Compared to the AMOC (Figure 5a,c), the AMV is represented by all simulations with less uncertainty and with less differences between the simulations.

The predictability of the AMV over the time period 1961–2013 in terms of correlation with observations from HadISST (Rayner et al., 2003) strongly depends on the assimilation method in lead years 2 to 5 (Figure 6b). Here, AMV is predicted best by the hindcasts initialized with oceanic EnKF assimilation. Hindcasts initialized by atmospheric nudging only and oceanic anomaly nudging predict the AMV significantly better than the historical ensemble, too. The AMV prediction skill in the lead years 2 to 5 of the hindcasts initialized by full-value nudging is strongly decreased due to the initialization shock described in Kröger et al. (2018). It is worth noting that for lead years 6 to 10, hindcasts initialized by either oceanic nudging show consistently higher skill than the other prediction systems. Skill of the hindcasts initialized by oceanic EnKF assimilation drops below the one of the historical ensemble. The differences in AMV predictability stand in contrast to the similarities in the representation of the AMV variability over time, pointing toward the importance of the interannual timing of the AMV due to the initialization process.

Both AMV and AMOC predictability (Figure 6) show at least a 5-year prediction horizon with a possible extension up to 10 years in case of the recovered AMV skill in the predictions initialized by oceanic nudging. For both parameters, the assimilation method strongly influences the predictability, in particular on lead years 2 to 5. On these lead times, methods with a less restricted large-scale atmosphere–ocean feedback—atmospheric nudging alone, and supplemented with oceanic EnKF assimilation—show generally better predictability.

6 | PREDICTABILITY OF SPG SST

The interannual to decadal variability of the AMOC determines large parts of the variability in the ocean heat transport in the North Atlantic from subtropical to subpolar latitudes on these time scales. In earlier versions of MPI-ESM, AMOC variability was linked with North Atlantic SST (Latif, Collins, Pohlmann, & Keenlyside, 2006) as well as European air surface temperature and precipitation (Pohlmann, Sienz, & Latif, 2006). In MPI-ESM-LR predictions of the whole 20th century, Borchert et al. (2018) found that North Atlantic SST is influenced by the Atlantic northward ocean heat transport on the time scale of 3–10 years, that is, phases of strong heat transport result in warm SST anomalies in the North Atlantic SPG and cold SST anomalies in the Gulf stream and North Atlantic current (NAC). We therefore expect that the different atmosphere–ocean impacts realized in our initializations not only lead to different representation and predictability of the AMOC, but ultimately also to differences in the predictability of North Atlantic SST in the investigated prediction systems (Figure 7).

We analyze prediction skill of North Atlantic SST in terms of correlation with HadISST near observational data (Rayner et al., 2003) over the time period 1961–2013. Over this period, the historical ensemble already shows significant prediction skill in many parts of the North Atlantic. Yet, in the SPG and the NAC, which are both strongly connected to the AMOC, prediction skill is low (Figure 7a).

The different atmosphere–ocean impact allowed in our assimilations determines if our initializations lead to qualitatively higher prediction quality, that is, retaining areas with significant correlation skill from the uninitialized historical ensemble like the Nordic Seas, and improve areas with below significance correlation skill in the historical ensemble such as the SPG and NAC (left column in Figure 7, differences in correlation in right column of Figure 7). Nudging to atmospheric reanalysis data alone improves skill in the NAC in relation to the historical ensemble. The oceanic EnKF additionally improves prediction skill in the SPG leading to significant skill in the Labrador Sea and Irminger Sea deep convection zones. In contrast, improvements by any oceanic nudging during assimilation are not as large as with atmospheric nudging alone. This effect is weak for oceanic anomaly nudging but strong for oceanic full-value nudging.

Inconsistencies between MPI-ESM-LR, the reanalysis data for the atmosphere, and the reanalysis data for the ocean impact the prediction skill of SST. In the full-value nudging approach, these inconsistencies not only lead to an initialization shock in the AMOC but also to an unbalanced heat budget on interannual to decadal time scales (Kröger et al., 2018). As a result, prediction skill in oceanic heat content (not shown) and SST (lower row in Figure 7) is decreased, the positive impact of initialization is more than counteracted. In contrast, in MPI-ESM-LR, both atmospheric nudging alone and EnKF assimilation of oceanic observations lead to a consistent response in AMOC and North Atlantic SSTs, the initialization effect on prediction skill is positive.

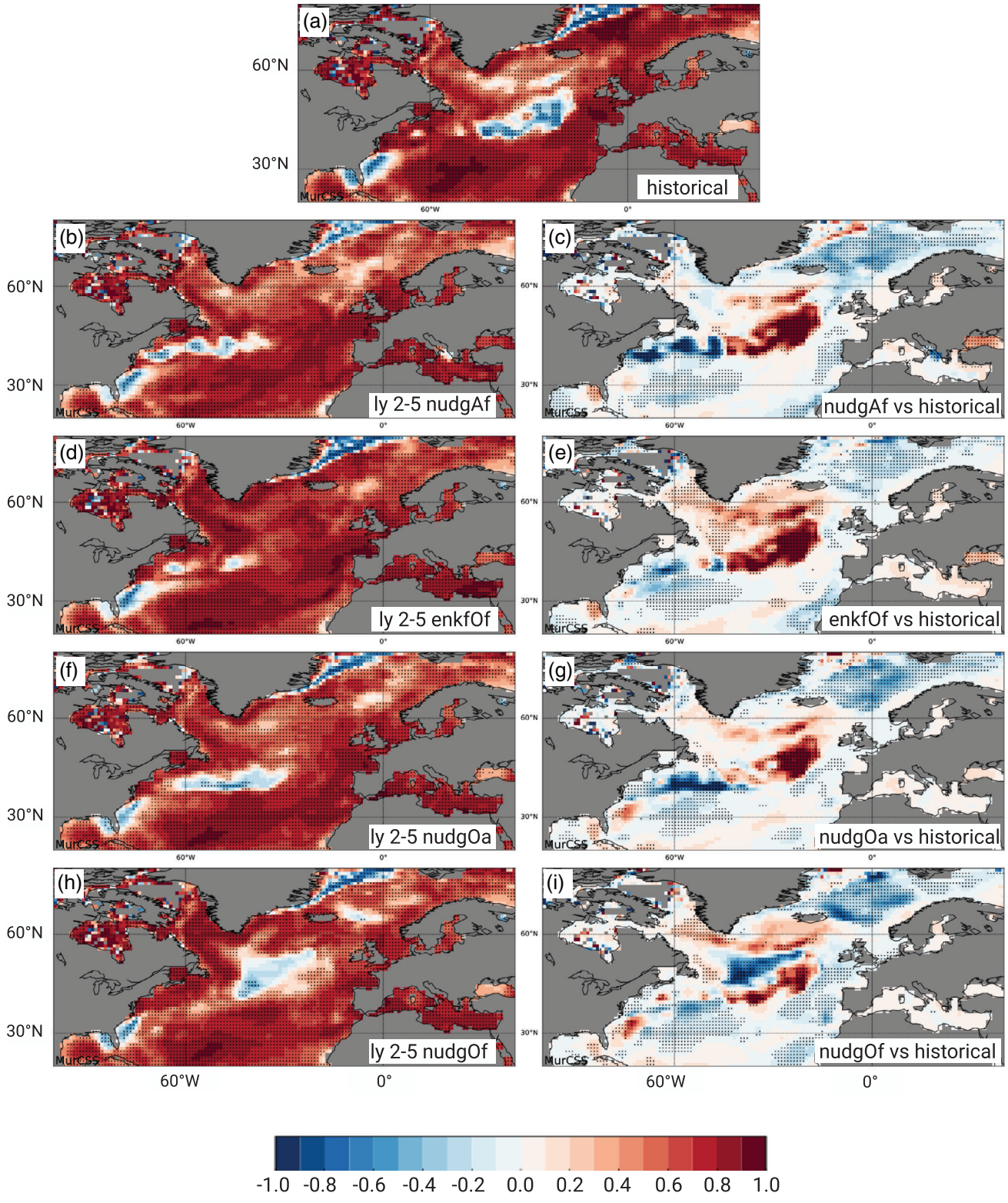

FIGURE 7 Prediction skill for sea surface temperature in terms of correlation with HadISST near observational data (Rayner et al., 2003) in the period 1961–2013 is already high in the uninitialized historical ensemble for large parts of the North Atlantic (a), which are dominated by a long-term trend. Prediction skill is low in areas without a dominant trend: the subpolar gyre and the North Atlantic current. In these areas, initialized hindcast shows partly improved skill in lead years 2–5 depending on the assimilation method: absolute correlation on the left, differences in correlation to the historical ensemble on the right. Atmospheric nudging alone (nudgAf, b,c) improves the lead years 2–5 prediction skill for the North Atlantic current region. The oceanic ensemble Kalman filter (EnKF) (enkfOf, d,e) additionally improves the western part of the subpolar gyre, whereas anomaly nudging to reanalysis data (nudgOa, f,g) results in no additional improvements and full-value nudging to reanalysis data (nudgOf, h,i) even counteracts the positive impact of atmospheric nudging and leads to deterioration of correlations in the southern part of the subpolar gyre

7 | CONCLUSIONS

In this study, we reviewed how the restriction of the large-scale atmosphere–ocean feedback during assimilation is linked with changes in the interannual to decadal prediction quality of North Atlantic SSTs (SPG and AMV) and the representation of the variability of the AMOC over the time period 1961–2013.

We assessed the quality of the prediction systems with respect to the uninitialized historical ensemble in a combined quantitative and qualitative way: within the region of interest, the initialized predictions should retain enough quality in areas where the uninitialized simulation shows already high prediction quality, but should increase quality in areas where the uninitialized simulation shows low prediction quality. For example, in the North Atlantic region, variability of SSTs is already well captured by the uninitialized simulation in many areas, for example, the Nordic Seas, with the exception of the SPG. The initialized predictions show improved quality for SSTs in the SPG, while retaining enough of the prediction quality of the uninitialized simulation in all other areas.

In our prediction suite, a less restricted and therefore well-preserved large-scale atmosphere–ocean feedback during assimilation leads to initializations, which simultaneously honor both the observed state and the model's free state. As a result, the prediction quality of North Atlantic SSTs is higher for initializations with a well-preserved large-scale atmosphere–ocean feedback than for initializations with little or no preservation of the large-scale atmosphere–ocean feedback. This leads to increased prediction quality for SSTs in the SPG and for the AMV. In addition, we find that the AMOC is sensitive to the atmosphere–ocean impact during assimilation and preserves the assimilation state on time scales of at least 5 years. Due to this memory, a careful initialization of the AMOC seems mandatory to tap the full prediction potential of our ESM in the North Atlantic.

We conclude that a well-preserved large-scale atmosphere–ocean feedback during assimilation allows for an initialization of the ESM consistent with both atmospheric and oceanic observations. In the North Atlantic, the quality of predictions initialized with a well-preserved large-scale atmosphere–ocean feedback is increased when compared to initializations where the large-scale atmosphere–ocean feedback is not preserved. This difference in prediction quality cannot be measured by the closeness of the assimilation to the observations alone.

ACKNOWLEDGMENTS

We thank Holger Pohlmann, Leonard Borchert, and Vimal Koul for discussing the results of our study as well as the manuscript. Special thanks to Wolfgang A. Müller and the MiKlip central prediction and central evaluation teams for their efforts in setting up and evaluating a decadal prediction framework with MPI-ESM. We thank Kameswarrao Modali and Helmuth Haak for technical help with MPI-ESM, and Lars Nerger for providing the Parallel Data Assimilation Framework for the use of the EnKF with MPI-ESM. We further thank three anonymous reviewers and the editor Eduardo Zorita for their constructive comments. Sea surface temperature data from HadISST and EN4 oceanic profile data have been retrieved through www.metoffice.gov.uk/hadobs, data for the RAPID-MOCHA array have been retrieved via http://www.rapid.ac.uk/rapidmoc/. Analysis for Figure 7 was produced with the MurCSS tool (Illing, Kadow, Oliver, & Cubasch, 2014). All simulation data are stored through MiKlip at the DKRZ archive and can be made accessible upon request. The model simulations were performed at the German Climate Computing Centre (DKRZ), under project 801: "MiKlip II Module A: Determination of initial conditions and initialization," and under project 807: "MiKlip II Module D – Synthesis."

CONFLICT OF INTERESTS

The authors have declared no conflicts of interest for this article.

AUTHOR CONTRIBUTIONS

Sebastian Brune: Conceptualization; formal analysis; investigation; visualization; writing-original draft; writing-review and editing. **Johanna Baehr**: Conceptualization; formal analysis; investigation; supervision; visualization; writing-original draft, review, and editing.

FURTHER READING

A summary of recent efforts on coupled data assimilation has been published in Penny et al. (2017), a comprehensive review of assimilation methods is presented in Carrassi, Bocquet, Bertino, and Evensen (2018). The AMOC is the topic of the extensive review of Buckley and Marshall (2016). The plans for the decadal climate prediction project (DCPP) within the World Climate Research Programme are outlined in Boer et al. (2016) and Eyring et al. (2016).

ORCID

Sebastian Brune https://orcid.org/0000-0001-7794-5465

REFERENCES

Anderson, J. L., Hoar, T., Raeder, K., Liu, H., Collins, N., Torn, R., & Avellano, A. (2009). The data assimilation research testbed: A community facility. *Bulletin of the American Meteorological Society*, *90*(9), 1283–1296.

Baehr, J. (2010). Influence of the 26°N RAPID-MOCHA array and Florida current cable observations on the ECCO-GODAE state estimate. *Journal of Physical Oceanography*, *40*(5), 865–879.

Balmaseda, M. A., Mogensen, K., & Weaver, A. T. (2013). Evaluation of the ECMWF Ocean reanalysis system ORAS4. *Quarterly Journal of the Royal Meteorological Society*, *139*(674), 1132–1161.

Bjerknes, J. (1964). Atlantic air-sea interaction. In *Advances in Geophysics* (Vol. 10, pp. 1–82). New York: Academic Press.

Boer, G. J., Smith, D. M., Cassou, C., Doblas-Reyes, F., Danabasoglu, G., Kirtman, B., ... Eade, R. (2016). The decadal climate prediction project (DCPP) contribution to CMIP6. *Geoscientific Model Development*, *9*(10), 3751–3777.

Borchert, L., Düsterhus, A., Brune, S., & Baehr, J. (2019). Forecast-oriented assessment of decadal hindcast skill for North Atlantic SST. *Geophysical Research Letters*, *46*(20), 11444–11454.

Borchert, L. F., Müller, W. A., & Baehr, J. (2018). Atlantic Ocean heat transport influences interannual-to-decadal surface temperature predictability in the North Atlantic region. *Journal of Climate*, *31*(17), 6763–6782.

Branstator, G., & Teng, H. (2012). Potential impact of initialization on decadal predictions as assessed for CMIP5 models. *Geophysical Research Letters*, *39*(12), 1–5.

Broecker, W. S. (1997). Thermohaline circulation, the Achilles heel of our climate system: Will man-made CO2 upset the current balance? *Science*, *278*(5343), 1582–1588.

Brune, S., Düsterhus, A., Pohlmann, H., Müller, W. A., & Baehr, J. (2018). Time dependency of the prediction skill for the North Atlantic subpolar gyre in initialized decadal hindcasts. *Climate Dynamics*, *51*(5), 1947–1970.

Brune, S., Nerger, L., & Baehr, J. (2015). Assimilation of oceanic observations in a global coupled earth system model with the SEIK filter. *Ocean Modelling*, *96*, 254–264.

Buckley, M. W., & Marshall, J. (2016). Observations, inferences, and mechanisms of the Atlantic meridional overturning circulation: A review. *Reviews of Geophysics*, *54*(1), 5–63.

Carrassi, A., Bocquet, M., Bertino, L., & Evensen, G. (2018). Data assimilation in the geosciences: An overview of methods, issues, and perspectives. *WIREs: Climate Change*, *9*(5), e535.

Clement, A., Bellomo, K., Murphy, L. N., Cane, M. A., Mauritsen, T., Rädel, G., & Stevens, B. (2015). The Atlantic multidecadal oscillation without a role for ocean circulation. *Science*, *350*(6258), 320–324.

Clement, A., Cane, M. A., Murphy, L. N., Bellomo, K., Mauritsen, T., & Stevens, B. (2016). Response to comment on "The Atlantic multidecadal oscillation without a role for ocean circulation". *Science*, *352*(6293), 1527–1527.

Collins, M., & Sinha, B. (2003). Predictability of decadal variations in the thermohaline circulation and climate. *Geophysical Research Letters*, *30*(6), 1–4.

Counillon, F., Bethke, I., Keenlyside, N. S., Bentsen, M., Bertino, L., & Zheng, F. (2014). Seasonal-to-decadal predictions with the ensemble Kalman filter and the Norwegian earth system model: A twin experiment. *Tellus A*, *66*, 1–21.

Cox, P., & Stephenson, D. (2007). A changing climate for prediction. *Science*, *317*(5835), 207–208.

Cunningham, S. A., Kanzow, T., Rayner, D., Baringer, M. O., Johns, W. E., Marotzke, J., ... Bryden, H. L. (2007). Temporal variability of the Atlantic meridional overturning circulation at 26.5°N. *Science*, *317*(5840), 935–938.

Danabasoglu, G., Yeager, S. G., Kim, W. M., Behrens, E., Bentsen, M., Bi, D., ... Yashayaev, I. (2016). North Atlantic simulations in Coordinated Ocean-ice reference experiments phase II (CORE-II). Part II: Inter-annual to decadal variability. *Ocean Modelling*, *97*, 65–90.

Dee, D. P., Uppala, S. M., Simmons, A. J., Berrisford, P., Poli, P., Kobayashi, S., ... Vitart, F. (2011). The ERA-Interim reanalysis: Configuration and performance of the data assimilation system. *Quarterly Journal of the Royal Meteorological Society*, *137*(656), 553–597.

Delworth, T. L., Manabe, S., & Stouffer, R. J. (1993). Interdecadal variations of the thermohaline circulation in a coupled ocean-atmosphere model. *Journal of Climate*, *6*(11), 1993–2011.

Doblas-Reyes, F. J., Andreu-Burillo, I., Chikamoto, Y., García-Serrano, J., Guemas, V., Kimoto, M., ... van Oldenborgh, G. J. (2013). Initialized near-term regional climate change prediction. *Nature Communications*, *4*, 1715.

Escudier, R., Mignot, J., & Swingedouw, D. (2013). A 20-year coupled ocean-sea ice-atmosphere variability mode in the North Atlantic in an AOGCM. *Climate Dynamics*, *40*(3), 619–636.

Evensen, G. (1994). Sequential data assimilation with a nonlinear quasi-geostrophic model using Monte Carlo methods to forecast error statistics. *Journal of Geophysical Research*, *99*(C5), 10143–10162.

Eyring, V., Bony, S., Meehl, G. A., Senior, C. A., Stevens, B., Stouffer, R. J., & Taylor, K. E. (2016). Overview of the coupled model intercomparison project phase 6 (CMIP6) experimental design and organization. *Geoscientific Model Development*, *9*(5), 1937–1958.

Flato, G., Marotzke, J., Abiodun, B., Braconnot, P., Chou, S. C., Collins, W., ... Rummukainen, M. (2013). *Evaluation of climate models* (pp. 741–882). Cambridge: Cambridge University Press.

Frankignoul, C., Czaja, A., & L'Heveder, B. (1998). Air-Sea feedback in the North Atlantic and surface boundary conditions for ocean models. *Journal of Climate*, *11*(9), 2310–2324.

Frankignoul, C., Kestenare, E., Botzet, M., Carril, A. F., Drange, H., Pardaens, A., ... Sutton, R. (2004). An intercomparison between the surface heat flux feedback in five coupled models, COADS and the NCEP reanalysis. *Climate Dynamics*, *22*(4), 373–388.

García-Serrano, J., Guemas, V., & Doblas-Reyes, F. J. (2015). Added-value from initialization in predictions of Atlantic multi-decadal variability. *Climate Dynamics*, *44*(9), 2539–2555.

Giorgetta, M. A., Jungclaus, J., Reick, C. H., Legutke, S., Bader, J., Böttinger, M., ... Stevens, B. (2013). Climate and carbon cycle changes from 1850 to 2100 in MPI-ESM simulations for the coupled model Intercomparison project phase 5. *Journal of Advances in Modeling Earth Systems*, *5*(3), 572–597.

Good, S. A., Martin, M. J., & Rayner, N. A. (2013). EN4: Quality controlled ocean temperature and salinity profiles and monthly objective analyses with uncertainty estimates. *Journal of Geophysical Research*, *118*(12), 6704–6716.

Griffies, S. M., & Bryan, K. (1997). Predictability of North Atlantic multidecadal climate variability. *Science*, *275*(5297), 181–184.

Grötzner, A., Latif, M., Timmermann, A., & Voss, R. (1999). Interannual to decadal predictability in a coupled ocean-atmosphere general circulation model. *Journal of Climate*, *12*(8), 2607–2624.

Gulev, S. K., Latif, M., Keenlyside, N., Park, W., & Koltermann, K. P. (2013). North Atlantic Ocean control on surface heat flux on multidecadal timescales. *Nature*, *499*, 464–467.

Hasselmann, K. (1976). Stochastic climate models Part I. Theory. *Tellus*, *28*(6), 473–485.

Hazeleger, W., Wouters, B., van Oldenborgh, G. J., Corti, S., Palmer, T., Smith, D., ... von Storch, J.-S. (2013). Predicting multiyear North Atlantic Ocean variability. *Journal of Geophysical Research*, *118*(3), 1087–1098.

Hoke, J. E., & Anthes, R. A. (1976). The initialization of numerical models by a dynamic-initialization technique. *Monthly Weather Review*, *104*(12), 1551–1556.

Houtekamer, P. L., & Zhang, F. (2016). Review of the ensemble Kalman filter for atmospheric data assimilation. *Monthly Weather Review*, *144*(12), 4489–4532.

Illing, S., Kadow, C., Oliver, K., & Cubasch, U. (2014). MurCSS: A tool for standardized evaluation of decadal Hindcast systems. *Journal of Open Research Software*, *2*(1), 1–3.

Kanzow, T., Cunningham, S. A., Rayner, D., Hirschi, J. J.-M., Johns, W. E., Baringer, M. O., ... Marotzke, J. (2007). Observed flow compensation associated with the MOC at 26.5°N in the Atlantic. *Science*, *317*(5840), 938–941.

Karspeck, A., Yeager, S., Danabasoglu, G., & Teng, H. (2015). An evaluation of experimental decadal predictions using CCSM4. *Climate Dynamics*, *44*, 907–923.

Karspeck, A. R., Stammer, D., Köhl, A., Danabasoglu, G., Balmaseda, M., Smith, D. M., ... Rosati, A. (2017). Comparison of the Atlantic meridional overturning circulation between 1960 and 2007 in six ocean reanalysis products. *Climate Dynamics*, *49*(3), 957–982.

Keenlyside, N. S., & Ba, J. (2010). Prospects for decadal climate prediction. *WIREs: Climate Change*, *1*(5), 627–635.

Keenlyside, N. S., Latif, M., Jungclaus, J., Kornblueh, L., & Roeckner, E. (2008). Advancing decadal-scale climate prediction in the North Atlantic sector. *Nature*, *453*(7191), 84–88.

Kröger, J., Müller, W. A., & von Storch, J.-S. (2012). Impact of different ocean reanalyses on decadal climate prediction. *Climate Dynamics*, *39*(3–4), 795–810.

Kröger, J., Pohlmann, H., Sienz, F., Marotzke, J., Baehr, J., Köhl, A., ... Müller, W. A. (2018). Full-field initialized decadal predictions with the MPI earth system model: An initial shock in the North Atlantic. *Climate Dynamics*, *51*(7), 2593–2608.

Lakshmivarahan, S., & Lewis, J. M. (2013). *Nudging Methods: A Critical Overview, pages 27–57*. Berlin and Heidelberg, Germany: Springer.

Latif, M., & Barnett, T. P. (1994). Causes of decadal climate variability over the North Pacific and North America. *Science*, *266*(5185), 634–637.

Latif, M., Collins, M., Pohlmann, H., & Keenlyside, N. (2006). A review of predictability studies of Atlantic sector climate on decadal time scales. *Journal of Climate*, *19*(23), 5971–5987.

Lei, L., & Hacker, J. P. (2015). Nudging, ensemble, and nudging ensembles for data assimilation in the presence of model error. *Monthly Weather Review*, *143*(7), 2600–2610.

Manabe, S., & Bryan, K. (1969). Climate calculations with a combined ocean-atmosphere model. *Journal of the Atmospheric Sciences*, *26*(4), 786–789.

Mantua, N. J., Hare, S. R., Zhang, Y., Wallace, J. M., & Francis, R. C. (1997). A Pacific interdecadal climate oscillation with impacts on Salmon production. *Bulletin of the American Meteorological Society*, *78*(6), 1069–1080.

Marini, C., Polkova, I., Köhl, A., & Stammer, D. (2016). A comparison of two ensemble generation methods using oceanic singular vectors and atmospheric lagged initialization for decadal climate prediction. *Monthly Weather Review*, *144*(7), 2719–2738.

Marotzke, J., Müller, W. A., & Vamborg, F. S. E. (2016). MiKlip: A National Research Project on decadal climate prediction. *Bulletin of the American Meteorological Society*, *97*(12), 2379–2394.

Matei, D., Baehr, J., Jungclaus, J. H., Haak, H., Müller, W. A., & Marotzke, J. (2012). Multiyear prediction of monthly mean Atlantic meridional overturning circulation at 26.5°N. *Science*, *335*(6064), 76–79.

McCarthy, G. D., Joyce, T. M., & Josey, S. A. (2018). Gulf stream variability in the context of quasi-decadal and multidecadal Atlantic climate variability. *Geophysical Research Letters*, *45*(20), 11,257–11,264.

Meehl, G. A., Goddard, L., Boer, G., Burgman, R., Branstator, G., Cassou, C., ... Yeager, S. (2014). Decadal climate prediction: An update from the trenches. *Bulletin of the American Meteorological Society*, *95*(2), 243–267.

Menary, M. B., Hodson, D. L. R., Robson, J. I., Sutton, R. T., & Wood, R. A. (2015). A mechanism of internal decadal Atlantic Ocean variability in a high-resolution coupled climate model. *Journal of Climate*, *28*(19), 7764–7785.

Msadek, R., Delworth, T. L., Rosati, A., Anderson, W., Vecchi, G., Chang, Y.-S., ... Zhang, S. (2014). Predicting a decadal shift in North Atlantic climate variability using the GFDL forecast system. *Journal of Climate*, *27*(17), 6472–6496.

Müller, V., Pohlmann, H., Düsterhus, A., Matei, D., Marotzke, J., Müller, W. A., ... Baehr, J. (2017). Hindcast skill for the Atlantic meridional overturning circulation at 26.5°N within two MPI-ESM decadal climate prediction systems. *Climate Dynamics*, *49*(9), 2975–2990.

Müller, W., Matei, D., Bersch, M., Jungclaus, J., Haak, H., Lohmann, K., ... Marotzke, J. (2015). A twentieth-century reanalysis forced ocean model to reconstruct the North Atlantic climate variation during the 1920s. *Climate Dynamics*, *44*(7–8), 1935–1955.

Nerger, L., & Hiller, W. (2013). Software for ensemble-based data assimilation systems—Implementation strategies and scalability. *Computers and Geosciences*, *55*, 110–118.

Ortega, P., Hawkins, E., & Sutton, R. (2011). Processes governing the predictability of the Atlantic meridional overturning circulation in a coupled GCM. *Climate Dynamics*, *37*(9), 1771–1782.

Penny, S. G., Akella, S., Alves, O., Bishop, C., Buehner, M., Chevallier, M., ... Wu, X. (2017). Coupled data assimilation for integrated Earth system analysis and prediction: Goals, challenges and recommendations. Technical report, WMO.

Persechino, A., Marsh, R., Sinha, B., Megann, A. P., Blaker, A. T., & New, A. L. (2012). Decadal-timescale changes of the Atlantic overturning circulation and climate in a coupled climate model with a hybrid-coordinate ocean component. *Climate Dynamics*, *39*(3), 1021–1042.

Pohlmann, H., Botzet, M., Latif, M., Roesch, A., Wild, M., & Tschuck, P. (2004). Estimating the decadal predictability of a coupled AOGCM. *Journal of Climate*, *17*(22), 4463–4472.

Pohlmann, H., Jungclaus, J. H., Köhl, A., Stammer, D., & Marotzke, J. (2009). Initializing decadal climate predictions with the GECCO oceanic synthesis: Effects on the North Atlantic. *Journal of Climate*, *22*(14), 3926–3938.

Pohlmann, H., Müller, W. A., Kulkarni, K., Kameswarrao, M., Matei, D., Vamborg, F. S. E., ... Marotzke, J. (2013). Improved forecast skill in the tropics in the new MiKlip decadal climate predictions. *Geophysical Research Letters*, *40*(21), 5798–5802.

Pohlmann, H., Sienz, F., & Latif, M. (2006). Influence of the multidecadal Atlantic meridional overturning circulation variability on European climate. *Journal of Climate*, *19*(23), 6062–6067.

Pohlmann, H., Smith, D. M., Balmaseda, M. A., Keenlyside, N. S., Masina, S., Matei, D., ... Rogel, P. (2013). Predictability of the mid-latitude Atlantic meridional overturning circulation in a multi-model system. *Climate Dynamics*, *41*(3), 775–785.

Polkova, I., Brune, S., Kadow, C., Romanova, V., Gollan, G., Baehr, J., ... Stammer, D. (2019). Initialization and ensemble generation for decadal climate predictions: A comparison of different methods. *Journal of Advances in Modeling Earth Systems*, *11*(1), 149–172.

Polkova, I., Köhl, A., & Stammer, D. (2014). Impact of initialization procedures on the predictive skill of a coupled ocean–atmosphere model. *Climate Dynamics*, *42*(11), 3151–3169.

Rayner, N. A., Parker, D. E., Horton, E. B., Folland, C. K., Alexander, L. V., Rowell, D. P., ... Kaplan, A. (2003). Global analyses of sea surface temperature, sea ice, and night marine air temperature since the late nineteenth century. *Journal of Geophysical Research*, *108*(D14), 1–37.

Robson, J. I., Ortega, P., & Sutton, R. (2016). A reversal of climatic trends in the North Atlantic since 2005. *Nature Geoscience*, *9*(7), 513–517.

Robson, J. I., Sutton, R. T., Lohmann, K., Smith, D. M., & Palmer, M. D. (2012). Causes of the rapid warming of the North Atlantic Ocean in the mid-1990s. *Journal of Climate*, *25*(12), 4116–4134.

Romanova, V., & Hense, A. (2017). Anomaly transform methods based on total energy and ocean heat content norms for generating ocean dynamic disturbances for ensemble climate forecasts. *Climate Dynamics*, *49*(3), 731–751.

Schlesinger, M. E., & Ramankutty, N. (1994). An oscillation in the global climate system of period 65-70 years. *Nature*, *367*, 723–726.

Servonnat, J., Mignot, J., Guilyardi, E., Swingedouw, D., Séférian, R., & Labetoulle, S. (2015). Reconstructing the subsurface ocean decadal variability using surface nudging in a perfect model framework. *Climate Dynamics*, *44*(1), 315–338.

Sluka, T. C., Penny, S. G., Kalnay, E., & Miyoshi, T. (2016). Assimilating atmospheric observations into the ocean using strongly coupled ensemble data assimilation. *Geophysical Research Letters*, *43*(2), 752–759 2015GL067238.

Smeed, D. A., McCarthy, G. D., Cunningham, S. A., Frajka-Williams, E., Rayner, D., Johns, W. E., ... Bryden, H. L. (2014). Observed decline of the Atlantic meridional overturning circulation 2004-2012. *Ocean Science*, *10*(1), 29–38.

Smith, D. M., Cusack, S., Colman, A. W., Folland, C. K., Harris, G. R., & Murphy, J. M. (2007). Improved surface temperature prediction for the coming decade from a global climate model. *Science*, *317*(5839), 796–799.

Smith, D. M., Eade, R., & Pohlmann, H. (2013). A comparison of full-field and anomaly initialization for seasonal to decadal climate prediction. *Climate Dynamics*, *41*(11–12), 3325–3338.

Srokosz, M., Baringer, M., Bryden, H., Cunningham, S., Delworth, T., Lozier, S., ... Sutton, R. (2012). Past, present, and future changes in the Atlantic meridional overturning circulation. *Bulletin of the American Meteorological Society*, *93*(11), 1663–1676.

Stommel, H. (1958). The abyssal circulation. *Deep Sea Research (1953)*, *5*(1), 80–82.

Tardif, R., Hakim, G. J., & Snyder, C. (2015). Coupled atmosphere–ocean data assimilation experiments with a low-order model and CMIP5 model data. *Climate Dynamics*, *45*(5), 1415–1427.

Taylor, K. E., Stouffer, R. J., & Meehl, G. A. (2012). An overview of CMIP5 and the experiment design. *Bulletin of the American Meteorological Society*, *93*(4), 485–498.

Tiedje, B., & Baehr, J. (2014). Limitations of the potential predictability of meridional mass and heat transports in the North Atlantic. *Geophysical Research Letters*, *41*(12), 4270–4276.

Uppala, S. M., Kållberg, P. W., Simmons, A. J., Andrae, U., Bechtold, V. D. C., Fiorino, M., ... Woollen, J. (2005). The ERA-40 re-analysis. *Quarterly Journal of the Royal Meteorological Society*, *131*(612), 2961–3012.

Volpi, D., Guemas, V., & Doblas-Reyes, F. J. (2017). Comparison of full field and anomaly initialisation for decadal climate prediction: Towards an optimal consistency between the ocean and sea-ice anomaly initialisation state. *Climate Dynamics*, *49*(4), 1181–1195.

Willis, J. K. (2010). Can in situ floats and satellite altimeters detect long-term changes in Atlantic Ocean overturning? *Geophysical Research Letters*, *37*(6), 1–5.

Wills, R. C. J., Armour, K. C., Battisti, D. S., & Hartmann, D. L. (2019). Ocean-atmosphere dynamical coupling fundamental to the Atlantic multidecadal oscillation. *Journal of Climate*, *32*(1), 251–272.

Yeager, S. G., & Robson, J. I. (2017). Recent Progress in understanding and predicting Atlantic decadal climate variability. *Current Climate Change Reports*, *3*(2), 112–127.

Zhang, R. (2008). Coherent surface-subsurface fingerprint of the Atlantic meridional overturning circulation. *Geophysical Research Letters*, *35*(20), 1–6.

Zhang, R., Sutton, R., Danabasoglu, G., Delworth, T. L., Kim, W. M., Robson, J., & Yeager, S. G. (2016). Comment on "The Atlantic multidecadal oscillation without a role for ocean circulation". *Science*, *352*(6293), 1527–1527.

How to cite this article: Brune S, Baehr J. Preserving the coupled atmosphere–ocean feedback in initializations of decadal climate predictions. *WIREs Clim Change*. 2020;11:e637. https://doi.org/10.1002/wcc.637